Chemistry & Biology, Vol. 11, 367–377, March, 2004, ©2004 Elsevier Science Ltd. All rights reserved. DOI 10.1016/j.chembiol.2004.02.015

Novel Heparan Sulfate Mimetic Compounds as Antitumor Agents

Keisuke Ishida,[1,2] Michal K. Wierzba,[1,3] Takayuki Teruya,[1,3] Siro Simizu,[1] and Hiroyuki Osada[1,3,*]
[1]Antibiotics Laboratory
RIKEN Discovery Research Institute
2-1 Hirosawa, Wako
Saitama 351-0198
[2]Hanno Research Center
Taiho Pharmaceutical Co., Ltd.
1-27 Misugidai, Hanno
Saitama 357-8527
[3]Graduate School of Science and Engineering
Saitama University
255 Shimo-okubo, Sakura-ku, Saitama
Saitama 338-8570
Japan

Summary

Heparan sulfate glycosaminoglycans (HSGAGs) are involved in tumor cell growth, adhesion, invasion, and migration, due to their interactions with various proteins. In this study, novel HSGAG-mimetic compounds (KI compounds) were designed and synthesized. As a result of cell-based assays, KI-105 was found to exert potent inhibitory activities against migration and invasion of human fibrosarcoma HT1080 cells. The present results indicate that a novel invasion/migration inhibitor, KI-105, can increase the adherence of HT1080 cells. It was conceivable that this cellular effect was caused by an increase in the amount of cell-surface HSGAGs and focal adhesions. Although further investigations are needed to decipher the molecular mechanism of KI-105, it is suggested that heparanase and Cdc42 are involved in its biological effects.

Introduction

Heparan sulfate glycosaminoglycans (HSGAGs) have been found to play regulatory roles in many biological functions that include both normal physiological processes (e.g., embryogenesis) [1] and pathological processes (e.g., tumorigenesis and metastasis) [2]. HSGAGs existing at the cell surface, as well as those in the extracellular matrix (ECM), are complex and highly sulfated polysaccharides that are ubiquitous in nearly all animals. In vivo, HSGAGs usually exist as protein conjugates referred to as heparan sulfate proteoglycans (HSPGs) [3]. Syndecans [4] and glypicans [5] are the two main groups of cell-surface HSPGs. Perlecan [6] and agrin [7] are the best-characterized HSPGs in the ECM.

HSGAGs on cell surface regulate signal transduction from the outside to the inside of tumor cells due to the interaction of HSGAGs with various growth factors such as bFGF [8] and VEGF [9]. Tumor-cell adhesion is also promoted by cell-surface HSGAGs acting as ligands for P-selectin and/or as coreceptors for integrins [10]. On the other hand, HSGAGs in the ECM act as a physical barrier against tumor metastasis, and they also function as storage sheds for various proteins [11]. Heparanase, a member of the endo-β-D-glucuronidase family, promotes tumor cell invasion by the degradation of HSGAGs in the ECM. Heparanase also promotes angiogenesis by the release of growth factors sequestered in HSGAGs such as bFGF and VEGF [12–15].

As regards structural characteristics, HSGAGs consist of regions with high levels of sulfation and epimerization (S domains), sequences with alternating N-acetylation and N-sulfation (NA/S domains), and unmodified domains that are mostly N-acetylated and contain little sulfate (unmodified domains) [16]. HSGAGs also consist of a repeating structure of the disaccharide unit of hexuronic acid (either iduronic acid or glucuronic acid) linked to a glucosamine. There are 48 possible disaccharide units that result from the sulfation of the 2-*O* position of uronic acid and the 6-*O* and 3-*O* positions of glucosamine and either the sulfation or acetylation of the N position of glucosamine. Even when HSGAGs consist of only six saccharides, there are 110,592 possible structures for these polysaccharides.

The enormous structural diversity of HSGAGs makes it possible for them to interact with a wide variety of proteins [17]. Such interactions make crucial contributions to the regulation of normal and pathological processes. In order to dissect a variety of the pathological roles of HSGAGs and develop novel antitumor agents, we designed novel HSGAG-mimetic compounds (KI compounds) using database search techniques; moreover, we took Lipinski's "Rule of Five" [18] and molecular dynamics calculations into consideration. Ease of organic synthesis was also a major concern when designing these mimetic compounds. Lipinski's "Rule of Five" is a simple mnemonic that states the characteristics of compounds with poor absorbability or permeability (there are more than 5 H-bond donors, 10 H-bond acceptors, the molecular weight is greater than 500, and the calculated Lop *P* is greater than 5). Lop *P* is the partition coefficient of *n*-octanol/water [19].

Results

Design and Synthesis of HSGAG-Mimetic Compounds

With the aim of developing antitumor agents, we focused on a number of the pathological roles of HSGAGs. First, we designed a novel mimetic structure for HSGAGs. Partial structures were searched based on the structure of the heparan sulfate (HS) disaccharide unit, HexUA-GlcNAc(6S) (where HexUA, GlcNAc, and 6S represent hexuronic acid, *N*-acethyl-D-glucosamine, and 6-*O*-sulfate, respectively), from an in-house database containing 50,000 compounds. Keeping ease of organic synthesis in mind, 80 compounds obtained from the database search were selected according to the Lip-

*Correspondence: hisyo@riken.jp

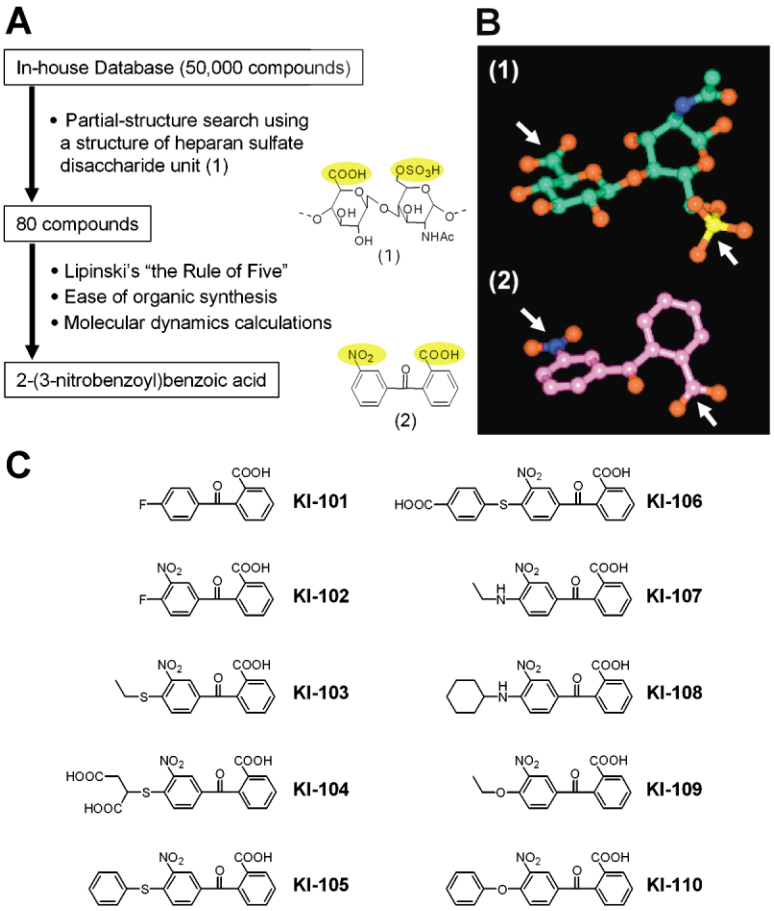

Figure 1. Discovery of Novel HSGAG-Mimetic Compounds (KI Compounds)

(A) Protocol used for the discovery of a novel HSGAG-mimetic structure. Chemical structure of a HS disaccharide unit (1), HexUA-GlcNAc(6S), and 2-(3-nitrobenzoyl)benzoic acid (2) are also shown.

(B) Energy-minimized structures of (1) and (2). The arrows show the anionic functional groups. The carbons of (1) and (2) are represented in green and pink, respectively. Oxygen, nitrogen, and sulfur are represented in red, blue, and yellow, respectively. The hydrogen atoms are not shown.

(C) Chemical structures of the KI compounds.

inski's "Rule of Five." The structures selected by this method were energy minimized by molecular dynamics calculation. The results of calculations were compared with those for HexUA-GlcNAc(6S). Finally, we selected 2-(3-nitrobenzoyl)benzoic acid as a core structure (Figure 1A). The energy-minimized structures of HexUA-GlcNAc(6S) and 2-(3-nitrobenzoyl)benzoic acid revealed that anionic groups, such as sulfate, carboxylic acid, and nitro functional groups, are able to locate in similar positions and directions (Figure 1B). HSGAG-mimetic compounds were synthesized using 2-(4-fluorobenzoyl)-benzoic acid (KI-101) as a starting material (Figure 1C). 2-(4-Fluoro-3-nitrobenzoyl)benzoic acid (KI-102) was obtained by the nitration of KI-101. KI-102 was treated with certain thiols, alcohols, and amines to give KI-103 through KI-110 (Figure 1C).

The Antagonistic Effects of KI Compounds in Cell-Based Assays

The antagonistic effects of KI compounds against invasion and migration of human fibrosarcoma HT1080 cells were assessed using Biocoat Matrigel Invasion Chamber and Cell Culture Insert. KI-105 inhibited both invasion and migration (Figure 2A). The inhibition percentages of migration and invasion by KI-105 at 100 μM were 62% and 69%, respectively. Heparan sulfate (HS) inhibited only invasion, and the inhibition at 100 μM of HS in disaccharide unit was 78%. A cytotoxic agent, paclitaxel, was used as a positive control. The inhibition of the migration and invasion resulting from treatment with paclitaxel at 100 nM were 82% and 96%, respectively.

The inhibitory activities exerted on the adhesion of HT1080 and HeLa cells to fibronectin were assessed using Biocoat fibronectin coat plates. The RGD peptide (GRGDNP, Gly-Arg-Gly-Asp-Asn-Pro), which inhibits cell adhesion to fibronectin [20], inhibited the adhesion of HeLa cells but not of HT1080 cells (Figure 2B). HS, paclitaxel, and the RGD control peptide (GRADSP, Gly-Arg-Ala-Asp-Ser-Pro; an inactive control for the RGD peptide) did not inhibit the adhesion of either type of cells to fibronectin. No KI compounds showed remarkable inhibitory activities as regards the adhesion of either type of cells to fibronectin (Figure 2B).

The inhibition of the growth of HT1080 cells induced by KI compounds was then assessed using the WST-8 assay (Figure 2C). Paclitaxel (100 nM) showed strong inhibitory activity after incubation of the cells at 37°C for 48 hr. However, it should be noted that at doses of up to 100 μM, none of KI compounds and HS possessed growth inhibition activity.

As a result of these cell-based assays, we found that KI-105 showed the most potent inhibition on tumor invasion and migration among KI compounds. The concentration dependency of KI-105 as regards the inhibition of migration and invasion of HT1080 cells is shown in

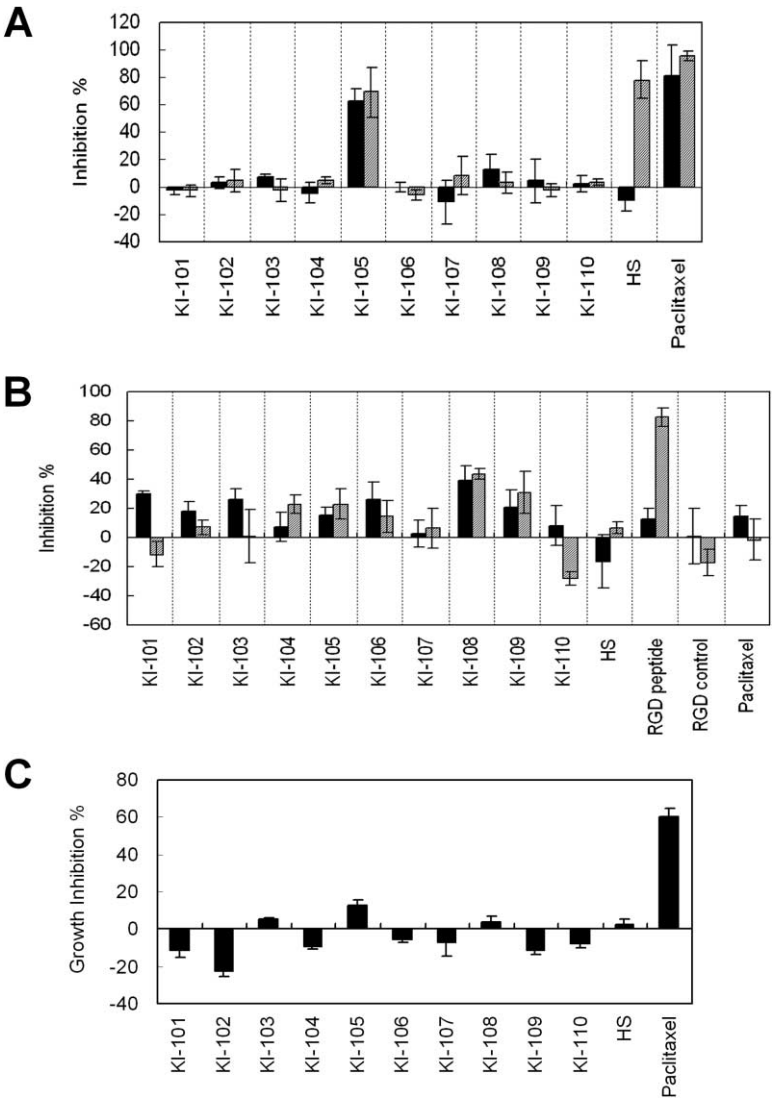

Figure 2. The Antagonistic Effects of KI Compounds in Cell-Based Assays

(A) Inhibition of migration and invasion of HT1080 cells by KI compounds. HT1080 cells (2.5×10^4 cells) were incubated with KI compounds (100 μM), HS (100 μM in disaccharide unit), or paclitaxel (100 nM) in chambers (membrane pore size, 8 μm) with or without Matrigel coating for 20 hr at 37°C. After removing the cells and the Matrigel from the upper side of the membrane, the cells that had moved to the lower side of the membrane were stained with crystal violet and counted. The results are the mean ± SD of three experiments. Black and hatched bars indicate migration (without Matrigel) and invasion (with Matrigel), respectively.

(B) Inhibition of adhesion of HT1080 and HeLa cells by KI compounds. HT1080 or HeLa cells (6×10^4 cells) were incubated with KI compounds (100 μM), HS (100 μM in disaccharide unit), RGD peptide (50 μM), RGD peptide control (50 μM), or paclitaxel (1 μM) for 1 hr at 37°C on fibronectin precoated 96-well plates. After washing the cells with PBS, adhering cells were stained with crystal violet and counted. The results are the mean ± SD of three experiments. Black and hatched bars indicate HT1080 and HeLa cells, respectively.

(C) Inhibition of cell growth of HT1080 cells by KI compounds. HT1080 cells (1×10^4 cells) were incubated for 12 hr at 37°C and were then treated with KI compounds (100 μM), HS (100 μM in disaccharide unit), or paclitaxel (100 nM) for 48 hr at 37°C. After incubation with WST-8 for 2 hr at 37°C, the absorbance at 405 nm was measured. The results are the mean ± SD of three experiments.

Figure 3. KI-105 inhibited migration and invasion equally (Figure 3A). The IC_{50} values of migration and invasion by KI-105 were 3.3 μM and 2.5 μM, respectively (Figure 3B). Tumor cell migration was also studied using an in vitro wound healing assay (Figure 3C). Confluent HT1080 cells were scratched (Figure 3Ca, time 0) and treated with chemicals for 20 hr. After treatment with vehicle, HT1080 cells migrated and covered a great area of the scratch (Figure 3Cb, control). On the other hand, KI-105 significantly inhibited the migration of HT1080 cells (Figures 3Cc–3Ce).

Effects of KI-105 on the Phenotype of HT1080 Cells

We measured the amount of cell-surface HSGAGs by immunofluorescence staining (Figure 4A). After treatment of HT1080 cells with KI-105 for 24 hr, the amount of cell-surface HSGAGs increased relative to that of control (Figures 4Ab and 4Ae). The merge picture of the control shows that HSGAGs were present not only at the cell surface but also in areas without cells (Figure 4Ac). This result indicates that the cells were peeled off by washing, and that ectocellular HSGAGs remained at the bottom. However, in the case of KI-105 treatment, the cells were not removed by washing (Figure 4Af). These results indicate that KI-105 not only augmented the amount of cell-surface HSGAGs but also augmented the incidence of cell adhesion.

The amount of cell-surface HSGAGs of HT1080 cells was also measured by flow cytometry (Figure 4B). Cell counts having high levels of log fluorescence intensity increased in the KI-105 treatment (Figure 4B, red line) as compared with nontreated cells (blue line). The maximum value of the log fluorescence intensity was moved from 80 to 500 by the KI-105 treatment.

The incidence of cell adhesion was also assessed by the adhesion assay described Experimental Procedures (Figure 4C). The adherent HT1080 cell numbers were significantly increased by KI-105 treatment for 24 hr against fibronectin, collagen IV, poly-Lys, and plastic (Figure 4Ca). Pictures of the adherent cells against fibronectin in treatment with vehicle or KI-105 for 24 hr are shown in Figures 4Cb and 4Cc, respectively.

Focal adhesions were visualized by anti-vinculin anti-

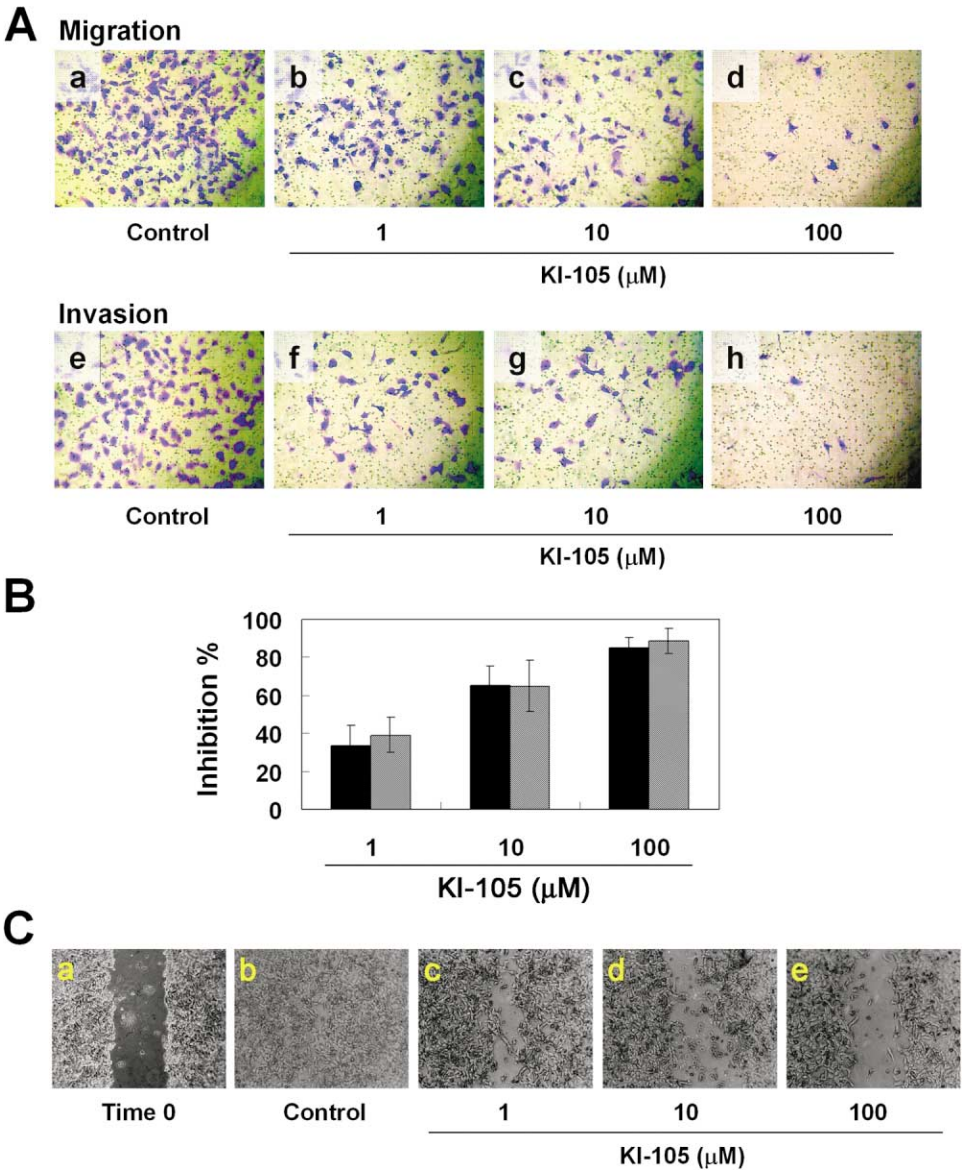

Figure 3. Effects of KI-105 on Migration and Invasion of HT1080 Cells

(A) Inhibition of migration and invasion of HT1080 cells by KI-105. The experimental procedure was same as that described in Figure 2A. HT1080 cells were incubated with vehicle or KI-105 at the indicated concentrations. Panels a–d show images of the migrated HT1080 cells treated with vehicle (a), 1 μM of KI-105 (b), 10 μM of KI-105 (c), or 100 μM of KI-105 (d) on the 8 μm pore membrane. Panels e–h show images of the invaded HT1080 cells treated with vehicle (e), 1 μM of KI-105 (f), 10 μM of KI-105 (g), or 100 μM of KI-105 (h) on the 8 μm pore membrane.

(B) Bar graph of the results of (A). The results are the mean ± SD of three experiments. Black and hatched bars indicate migration and invasion, respectively.

(C) Migration analysis by in vitro wound healing assay. After incubation of HT1080 cells (5×10^5 cells/6-well plate) for 24 hr, an artificial wound was created using P-10 pipette tip (a). The cells were treated with vehicle (b), 1 μM of KI-105 (c), 10 μM of KI-105 (d), or 100 μM of KI-105 (e) for 20 hr.

body, as vinculin localizes at focal adhesions. The number of focal adhesions was significantly increased by treatment with KI-105 for 24 hr (Figure 4De) in comparison with control (Figure 4Db). Focal adhesions were observed in the peripheral area of cells in the case of vehicle treatment (Figure 4Dc). However, focal adhesions were located not only at the peripheral area but also the inside area of cells in the case of KI-105 treatment (Figure 4Df). These results indicate that KI-105 augments the amount of cell-surface HSGAGs, adherence, and focal adhesions in HT1080 cells.

Effects of KI-105 on Several Proteins

We tested the inhibitory activities of KI-105 against several degradation enzymes, such as matrix metalloproteinases (MMPs), coagulant factors, and heparanase, because of their involvement in tumor invasion and migration (Table 1) [21–23]. KI-105 was found to possess

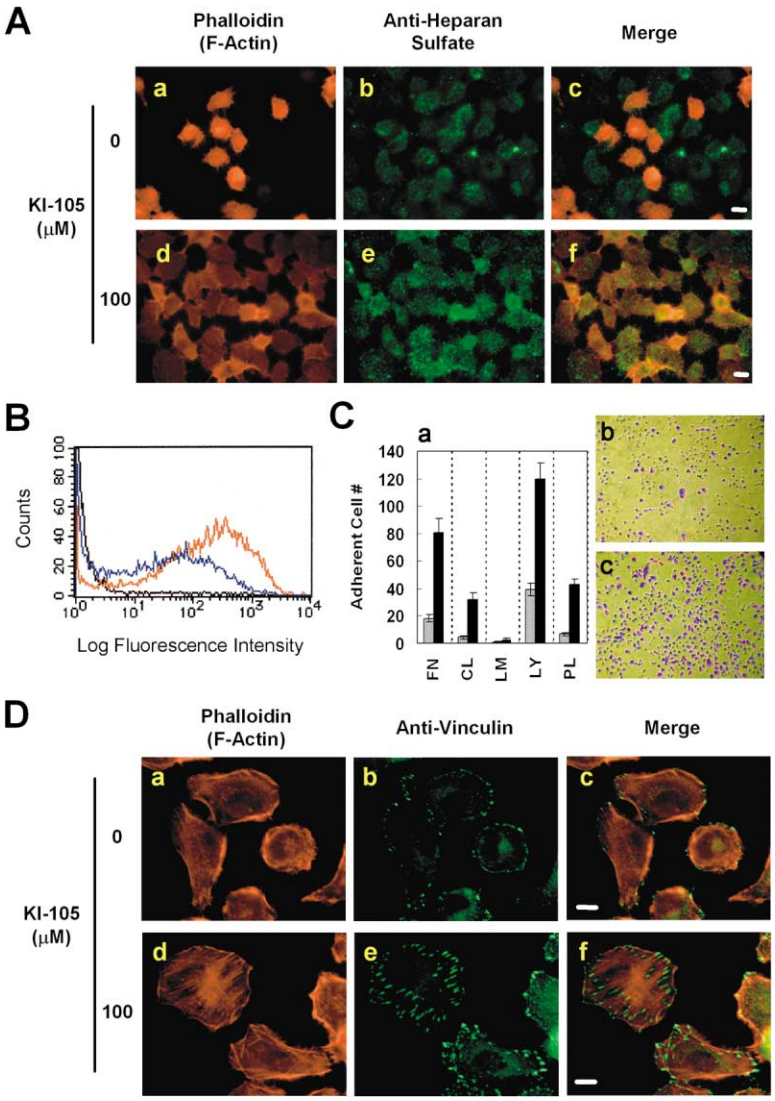

Figure 4. Effects of KI-105 on the Phenotype of HT1080 Cells

(A) Immunofluorescence staining of HT1080 cells. HT1080 cells were treated with vehicle (a, b, c) or 100 μM of KI-105 (d, e, f) for 24 hr. F-actin (red) and cell-surface HS (green) were stained with Alexa Fluor 568 Phalloidin and anti-HS antibody, respectively. White bars indicate 10 μm.

(B) FACS analysis of HT1080 cells. HT1080 cells were pretreated with vehicle for 48 hr. The cells were incubated with (blue line) or without (black line) anti-HS antibody and subsequently incubated with secondary antibody. HT1080 cells were pretreated with KI-105 (50 μM) for 48 hr. The cells were incubated with anti-HS antibody and incubated with secondary antibody (red line). The level of cell-surface HSGAGs expression was analyzed by flow cytometry.

(C) Adhesion assay of HT1080 cells. Panel a: HT1080 cells were incubated with vehicle or KI-105 (100 μM) for 20 hr on fibronectin (FN), collagen IV (CL), laminin (LM), poly-D-lysine (LY), or plastic (PL) precoated 35 mm dishes. After washing the cells with PBS, adherent cells were stained with crystal violet and counted. The results are the mean ± SD of three experiments. Hatched and black bars indicate vehicle or KI-105 treated HT1080 cells, respectively. Panels b and c show images of the adherent HT1080 cells treated with vehicle (b) or KI-105 (c) on fibronectin.

(D) Immunofluorescence staining of HT1080 cells. HT1080 cells were treated with vehicle (a, b, c) or 100 μM of KI-105 (d, e, f) for 20 hr. F-actin (red) and vinculin (green) were stained with Alexa Fluor 568 Phalloidin and anti-vinculin antibody, respectively. White bars indicate 10 μm.

heparanase inhibitory activity but did not inhibit the activity of MMP-2, MMP-9, collagenase, factor Xa, thrombin, trypsin, and urokinase-type plasminogen activator. The IC_{50} value of KI-105 against heparanase was 300 μM (Figure 5A). A correlation between the heparanase inhibitory properties of KI-105 and the cellular effect was assessed using an anti-heparanase antibody (Figure 5B). The invasion and migration of HT1080 cells were significantly inhibited by the anti-heparanase antibody treatment as compared with the normal mouse IgG treatment.

Table 1. The Inhibitory Activities of KI-105 against Several Degradation Enzymes

Enzyme	Inhibition Percentage[a]
MMP[b]-2 (human)	7.1 ± 7.2
MMP[b]-9 (human)	−21.2 ± 7.4
Collagenase (*Clostridium histolyticum*)	9.6 ± 4.1
Factor Xa (human)	0.1 ± 1.3
Thrombin (human)	−26.1 ± 9.2
Trypsin (human pancreas)	−4.3 ± 0.6
uPA[c] (human urine)	5.1 ± 6.2
Heparanase (human)	43.6 ± 8.6

[a] The concentration of KI-105 was 300 μM.
[b] Matrix metalloproteinase.
[c] Urokinase-type plasminogen activator.

The effect of KI-105 on several proteins implicated in cell-matrix adhesion and cell migration was evaluated by Western blotting (Figure 5C). The amount of the Rho-related small GTP binding protein Cdc42 was remarkably increased in the KI-105 treatment. The amount of paxillin was also increased slightly. However, amounts of other proteins assessed (Rac1, Rho, ILK, FAK, αPAK, NCK, phosphotyrosine, and α-tubulin) were not altered by KI-105 treatment.

Molecular Basis of KI-105

Novel heparan sulfate mimetic compound KI-105 was found to have weak inhibitory activity for heparanase and also found to increase the amount of the Rho-

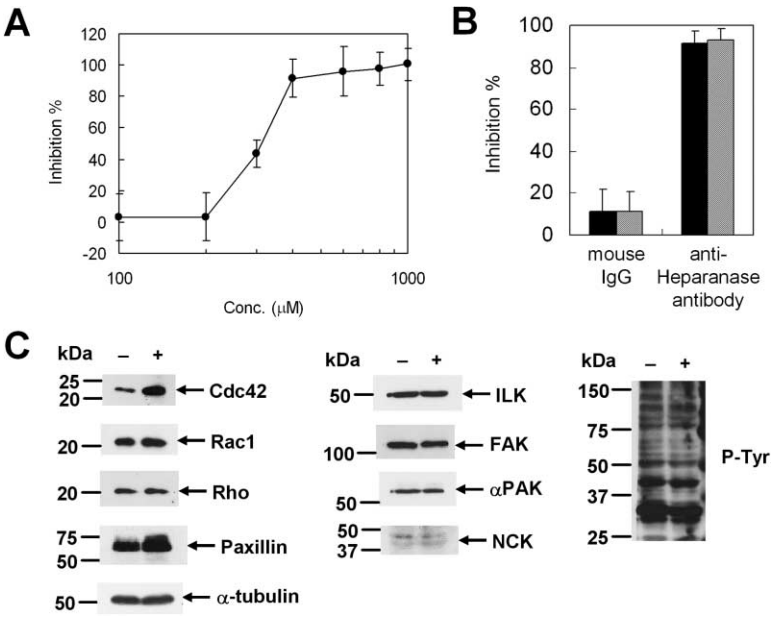

Figure 5. Effects of KI-105 on Several Proteins

(A) Dose-response curve of heparanase inhibition by KI-105. Cell lysate (2.0 mg/ml of protein) of HepG2-HP and HS (10 mg/ml in PBS, pH 6.2) were incubated with vehicle or KI-105 for 24 hr at 37°C. The reaction mixture was subjected to SDS-PAGE (20%). After electrophoresis, the gel was stained with alcian blue. The respective volumes of the bands were measured using an MD Scanning Imager equipped with MD ImageQuant Software Version 3.22 (Molecular Dynamics, Inc.) for quantification. The results are the mean ± SD of three experiments.

(B) Inhibition of migration and invasion of HT1080 cells by anti-heparanase antibody. The experimental procedure was the same as that described in Figure 2A. HT1080 cells were incubated with normal mouse IgG (67 μg/ml) or anti-heparanase antibody (42 μg/ml) for 20 hr. The results are the mean ± SD of three experiments. Black and hatched bars indicate migration and invasion, respectively.

(C) Western blotting analysis with specific antibodies. HT1080 cells were incubated with vehicle (−) or 100 μM of KI-105 (+) for 20 hr.

related small GTP binding protein Cdc42. The mechanism of how KI-105 increases the amount of Cdc42 has been unclear until the present. So, we have assessed the molecular basis of KI-105 by interaction with heparanase and comparison with a very similar inactive compound, KI-110.

The results of database searches and site-directed mutagenesis have suggested that mammalian heparanase is related to members of glycosyl hydrolase families 10, 39, and 51, which have been predicted to have $(\alpha/\beta)_8$ TIM-barrel folds [24]. 1,4-β-xylanase from *Penicillium simplicissimum* is a member of the glycosyl hydrolase family 10, and its X-ray structure has been determined. Therefore, homology modeling of heparanase was performed using the X-ray structure of 1,4-β-xylanase from *Penicillium simplicissimum* as a template. KI-105 was manually located at the active site, under consideration of the electrostatic interactions and hydrophobicity, and then the structure of the heparanase/KI-105 complex was energy minimized using molecular mechanics and dynamic calculations (Figure 6A). The complex was stabilized by electrostatic interactions between Arg303 and the carboxylic group of KI-105 and between Arg272 and the nitro group of the compound. π-π stacking between Phe229 and the thiophenol group of KI-105 was also observed.

The energy-minimized structure of KI-110 was obtained using the conformation of KI-105 in the heparanase/KI-105 complex as a starting structure. The difference between KI-105 and KI-110 was the direction of the benzene ring (Figures 6B and 6C). Torsion angles *A(1-2-3-4)* and *B(2-3-4-5)* of KI-105 were 75.8° and 10.1°, respectively. Torsion angles *A(1-2-3-4)* and *B(2-3-4-5)* represent the dihedral angles defined by the atoms *1*, *2*, *3*, *4*, and *5*, which are indicated in Figure 6B. Torsion angles *A(1-2-3-4)* and *B(2-3-4-5)* of KI-110 were 108.6° and −73.7°, respectively. The superimposed structures of KI-105 and KI-110 are also shown in Figure 6C.

Discussion

Most heparin or HS imitators are aimed at enhancing the inhibition of tumor metastasis, arteriosclerosis, and inflammation; they are most often sulfated oligosaccharides (e.g., heparin derivatives [25, 26], laminarin sulfate [27], and chitin derivatives [28]). There are many difficulties involved in the development of HSGAG-mimetic compounds, because HSGAGs carry out multiple functions and are difficult to synthesize. Thus, low molecular weight HSGAG mimics with high specificity that are easy to prepare are still needed. Some low molecular weight HSGAG mimics that are sulfated oligosaccharides have been reported to show antitumor activities. Phosphomannopentaose sulfate (PI-88) has been reported to significantly inhibit tumor growth, metastasis, and angiogenesis [29]. A pseudodisaccharide compound mimicking a unit of a HSGAG, designed as a heparanase inhibitor, was synthesized, and the inhibitory activity against tumor cell heparanase was measured (IC_{50} value of 58–63 μM) [30]. Such low molecular weight HSGAG mimics are saccharide-based structures, although KI compounds are not sugar-based compounds.

Novel HSGAG-mimetic compounds (KI compounds) were designed and synthesized in the present study. As a result of cell-based assays (i.e., migration, invasion, adhesion, and growth assays), KI-105 was found to possess potent inhibitory activities on the invasion and migration of HT1080 cells. The IC_{50} values of migration and invasion by KI-105 were 3.3 μM and 2.5 μM, respectively. The inhibitory activity of KI-105 on the migration of HT1080 cells was also confirmed using in vitro wound healing assay.

If the main mechanism of KI-105 is assumed to be a simple obstruction of the degradation of HSGAGs in the ECM, only the invasion and not the migration of HT1080 cells would be inhibited. Indeed, intact HS inhibited only the invasion of HT1080 cells. However, KI-105 inhibited

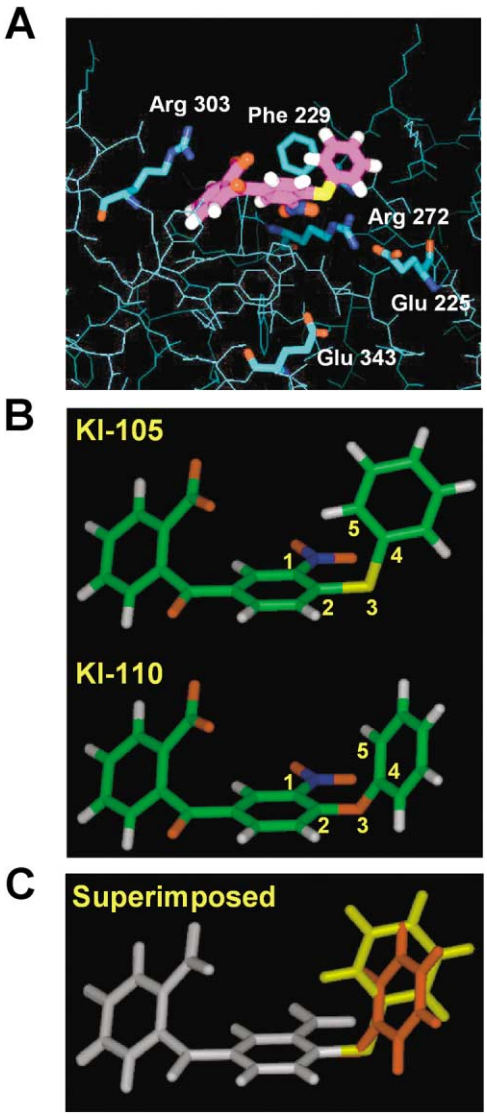

Figure 6. Molecular Basis of KI-105

(A) Modeled structure of a heparanase/KI-105 complex model. KI-105, active-site Glu residues, and the amino acid residues that interacted with KI-105 are indicated in boldface type. The atoms in KI-105 are represented in pink (carbon), white (hydrogen), red (oxygen), blue (nitrogen), and yellow (sulfur). The atoms in the amino acids, indicated in boldface type, are represented in sky blue (carbon), red (oxygen), and blue (nitrogen).

(B) Energy-minimized structures of KI-105 and KI-110. The atoms in KI-105 and KI-110 are represented in green (carbon), white (hydrogen), red (oxygen), blue (nitrogen), and yellow (sulfur). Yellow numbers are used for a definition of torsion angles.

(C) Superimposed structures of KI-105 and KI-110. Overlapped structure is represented in white. Thiophenol of KI-105 and phenol of KI-110 are represented in yellow and red, respectively.

both the invasion and the migration of HT1080 cells (Figure 2A). These results suggest that KI-105 inhibited the degradation of HSGAGs not only in the ECM but also on cell surface.

KI-105 treatment for 24 hr remarkably increased the adherence of HT1080 cells against fibronectin, collagen IV, poly-lysine, and plastic (Figure 4C), but treatment for 1 hr did not change the adherence (Figure 2B). So KI-105 was thought to change the character of HT1080 cells in 24 hr. KI-105 increased the number of focal adhesion of HT1080 cells (Figure 4D). It is unclear how the number of focal adhesion is augmented; however, KI-105 remarkably increased the amount of Cdc42 (Figure 5C). Cdc42 is a member of the Rho family GTPases and is well known to be involved in cell migration and formation of focal complexes [31, 32]. So an increase in the number of focal adhesion of HT1080 cells by KI-105 may be under Cdc42's control, but this assumption needs further investigation.

KI-105 (100 μM) moderately increased the amount of cell-surface HSGAGs on HT1080 cells (Figures 4A and 4B). KI-105 also showed moderate inhibition of heparanase (IC_{50} 300 μM, Figure 5A). Because only one heparanase cDNA sequence coding functional enzyme has been identified to date, heparanase has been considered a major enzyme that degrades HSGAGs in mammalian tissues [12–15] and human tumors [33]. Heparanase inhibition by KI-105 may correlate with an increase in the amount of cell-surface HSGAGs on HT1080 cells. Therefore, it is conceivable that the increase in cell-surface HSGAGs by KI-105 treatment was caused not by the enhancement of biosynthesis of HSGAGs but the inhibition of degradation of cell-surface HSGAGs by heparanase.

Heparanase is well known to be involved in tumor invasion and migration by two different mechanisms [12–15]. One is the degradation of HSPGs in the ECM, which is especially involved in invasion, because HSPGs are known to be physical barriers against the invasion of tumor cells. The other is the degradation of cell-surface HSPGs (e.g., syndecans), which is a key mechanism of cell spreading and migration. For example, syndecan-4 is known to be located at sites of cell-matrix adhesion [34], and it regulates cell spreading and migration in cooperation with integrins [35, 36]. Thus, the present findings indicating that heparanase inhibition by KI-105 results in inhibition of the invasion and migration of HT1080 cells are consistent with previous reports. The invasion and migration of HT1080 cells were also inhibited by the anti-heparanase antibody treatment (Figure 5B). This result supports a correlation between the heparanase inhibition and the invasion/migration inhibition.

Molecular modeling of the heparanase/KI-105 complex and comparison between KI-105 (active) and a very similar compound, KI-110 (inactive), revealed the molecular basis of KI-105. π-π stacking between Phe-229 and the thiophenol group of KI-105 was observed in the heparanase/KI-105 complex model (Figure 6A). The direction of the benzene ring of thiophenol (KI-105) and phenol (KI-110) groups was different (Figures 6B and 6C). Based on these results, it may be possible to discover more potent antimigratory agents using KI-105 as a lead compound.

Significance

During the past decade, HSGAGs have been recognized to play important roles in the biology of cancer, i.e., in tumorigenesis, tumor progression, and metas-

tasis. Because of the unique structural features of HSGAGs, which are highly sulfated oligosaccharides, it has been difficult to develop nonsaccharide-based HSGAG regulators with low molecular weight. Many known HSGAG regulators are derivatives of sulfated oligosaccharides. Here, we developed novel functional regulators of HSGAGs that do not have a saccharide-based structure. We selected 2-(3-nitrobenzoyl)benzoic acid by database searches with regard to Lipinski's "Rule of Five" and the ease of organic synthesis; molecular dynamics calculations were also carried out as part of the selection process. A novel invasion/migration inhibitor, KI-105, was identified among the 2-(3-nitrobenzoyl)benzoic acid derivatives (KI compounds), using cell-based assays (i.e., invasion, migration, adhesion, and growth assays). KI-105 was found to increase the adherence of HT1080 cells. The amount of cell-surface HSGAGs and focal adhesions were also increased by KI-105 treatment. To the best of our knowledge, this is the first report of a rationally designed and experimentally identified low molecular weight HSGAG-mimetic compound demonstrating potent inhibition of the various functions involved in oncogenic processes.

Experimental Procedures

General Methods

The melting points of the synthesized compounds were measured with a Yanagimoto micro melting point apparatus (Yanagimoto, Kyoto, Japan) and are presented here as uncorrected values. Proton NMR spectra were recorded on a JEOL JNM-EX270 spectrometer (JEOL, Tokyo, Japan) or on a Varian UNITY*plus* 500 spectrometer (Varian, Palo Alto, CA). The chemical shifts were expressed in δ units, using the solvent as an internal standard. The mass spectra were obtained on a JEOL JMS-SX102 spectrometer (JEOL, Tokyo, Japan). All compounds for biological assays were dissolved in DMSO.

Design and Computer Calculations

A HS disaccharide unit of HexUA-GlcNAc(6S) (where HexUA, GlcNAc, and 6S represent hexuronic acid, *N*-acethyl-D-glucosamine, and 6-*O*-sulfate, respectively) was used as a template structure. Focusing on carboxylic acid and sulfate groups, a partial structure search was carried out using the ISIS/Base (MDL Information Systems, San Leandro, CA) in combination with a two-dimensional structure database containing 50,000 compounds (i.e., both original and commercial compounds). The eighty compounds obtained were automatically converted to three-dimensional structures using in-house C programs, and then the structures were energy minimized with Discover3 module of InsightII (Accelrys, San Diego, CA). The energy minimization protocol was as follows: molecular mechanics, 200 steps; molecular dynamics, 200 fs at 800 K; molecular dynamics, 200 fs at 298 K; and molecular mechanics, 200 steps. The criteria for the selection of the HS mimics were the positions and directions of anionic groups (i.e., sulfate, carboxylic acid, and nitro functional groups) as well as the ease of organic synthesis and Lipinski's "Rule of Five" [18].

Chemicals

2-(4-fluorobenzoyl)benzoic acid, sodium ethanethioate, 1,4-dioxane, mercaptosuccinic acid, *N,N*-diisopropylethylamine (DIPEA), 4-mercaptobenzoic acid, ethylamine, cyclohexylamine, sodium ethoxide, and sodium phenoxide trihydrate were purchased from Aldrich Chemical Corp. (Milwaukee, WI). Fuming HNO_3, thiophenol, and alcian blue 8GX were purchased from Wako Pure Chemical Industries (Osaka, Japan). Paclitaxel was purchased from Sigma Chemical Co (St. Louis, MO). RGD peptide (GRGDNP) and RGD control peptide (GRADSP) were purchased from BIOMOL Research Laboratories (Plymouth Meeting, PA). HS sodium salt from bovine kidney was purchased from Seikagaku Corp (Tokyo, Japan).

Synthesis of Compounds

2-(4-Fluoro-3-Nitrobenzoyl)Benzoic Acid (KI-102)

A suspension of 11.0 g of 2-(4-fluorobenzoyl)benzoic acid (KI-101) in 30 ml of fuming HNO_3 was stirred at 4°C for 2 hr and at room temperature for 5 hr. The reaction mixture was poured into ice water and extracted with chloroform. The chloroform extract was washed with water, dried over anhydrous $MgSO_4$, and concentrated in vacuo. The residue was purified by a preparative medium pressure liquid chromatography (YAMAZEN Corp., Osaka, Japan) on silica gel (chloroform:methanol = 95:5). Yield, 22%; mp, 174–176°C; ^{1}H NMR (500 MHz, acetone-d_6) 7.49 (1H, d, J 7.5 Hz), 7.57 (1H, dd, J 8.5 Hz, 10.5 Hz), 7.69 (1H, dd, J 7.5 Hz, 7.5 Hz), 7.77 (1H, dd, J 7.5 Hz, 7.5 Hz), 8.01 (1H, ddd, J 2.0 Hz, 4.0 Hz, 8.5 Hz) 8.08 (1H, d, J 7.5 Hz), 8.34 (1H, dd, J 2.0 Hz, 7.5 Hz); MS (FAB, Neg) m/z 288 $(M-H)^-$; HRMS (FAB, Neg) $C_{14}H_7NO_5F$: calculated 288.0308, found m/z 288.0311 $(M-H)^-$.

2-(4-Ethylthio-3-Nitrobenzoyl)Benzoic Acid (KI-103)

A mixture of 76 mg of KI-102 and 28 mg of sodium ethanethioate in 2 ml of 1,4-dioxane was stirred at room temperature for 4 hr and was extracted with chloroform. The chloroform extract was purified by a preparative medium pressure liquid chromatography (YAMAZEN Corp.) on silica gel (chloroform). Yield, 61%; ^{1}H NMR (270 MHz, DMSO-d_6) 1.30 (3H, t, J 5.5 Hz), 3.10 (2H, q, J 5.5 Hz), 7.37 (1H, d, J 6.5 Hz), 7.61–7.81 (4H, m), 8.00 (1H, d, J 6.8 Hz), 8.27 (1H, br-s); MS (FAB, Neg) m/z 330 $(M-H)^-$; HRMS (FAB, Neg) $C_{16}H_{12}NO_5S$: calculated 330.0436, found m/z 330.0444 $(M-H)^-$.

2-[4-(1, 2-Dicarboxyethyl)Thio-3-Nitrobenzoyl]Benzoic Acid (KI-104)

A mixture of 100 mg of KI-102 and 52 mg of mercaptosuccinic acid and 45 mg of DIPEA in 2 ml of 1,4-dioxane was stirred at room temperature for 12 hr and was extracted with chloroform. The chloroform extract was purified by a preparative medium pressure liquid chromatography (YAMAZEN Corp.) on silica gel (chloroform:methanol = 95:5). Yield, 84%; ^{1}H NMR (270 MHz, DMSO-d_6) 2.81 (1H, dd, J 5.7 Hz, 17.3 Hz), 2.93 (1H, dd, J 7.9 Hz, 17.3 Hz), 4.47 (1H, dd, J 5.7 Hz, 7.9 Hz), 7.49 (1H, d, J 7.0 Hz), 7.69 (1H, ddd, J 1.4 Hz, 7.6 Hz, 7.6 Hz), 7.76 (1H, ddd, J 1.4 Hz, 7.6 Hz, 7.6 Hz), 7.87 (1H, d, J 8.4 Hz), 7.99 (1H, d, J 8.4 Hz), 8.01 (1H, d, J 7.0 Hz), 8.25 (1H, d, J 1.6 Hz); MS (FAB, Neg) m/z 418 $(M-H)^-$; HRMS (FAB, Neg) $C_{18}H_{12}NO_9S$: calculated 418.0233, found m/z 418.0249 $(M-H)^-$.

2-[3-Nitro-4-(Phenylthio)Benzoyl]Benzoic Acid (KI-105)

A mixture of 226 mg of KI-102 and 86 mg of thiophenol and 101 mg of DIPEA in 3 ml of 1,4-dioxane was stirred at room temperature for 12 hr and extracted with chloroform. The chloroform extract was purified by a preparative medium pressure liquid chromatography (YAMAZEN Corp.) on silica gel (chloroform:methanol = 95:5), and then purified by reversed-phase HPLC using a PEGASIL ODS column (4.6 × 250 mm, Senshu Scientific Co. Ltd., Tokyo, Japan) with 20%–100% CH_3CN (0.05% TFA). Yield, 33%; mp, 138-140°C; ^{1}H NMR (270 MHz, DMSO-d_6) 6.93 (1H, d, J 8.4 Hz), 7.45 (1H, d, J 7.3 Hz), 7.60–7.80 (8H, m), 8.01 (1H, d, J 7.3 Hz), 8.33 (1H, s), 13.35 (1H, br-s); MS (FAB, Neg) m/z 378 $(M-H)^-$; HRMS (FAB, Neg) $C_{20}H_{12}NO_5S$: calculated 378.0436, found m/z 378.0450 $(M-H)^-$.

2-[4-(4-Carboxyphenyl)Thio-3-Nitrobenzoyl]Benzoic Acid (KI-106)

A mixture of 217 mg of KI-102 and 117 mg of 4-mercaptobenzoic acid and 97 mg of DIPEA in 5 ml of 1,4-dioxane was stirred at room temperature for 12 hr and extracted with chloroform. The chloroform extract was purified by a preparative medium pressure liquid chromatography (YAMAZEN Corp.) on silica gel (chloroform:methanol = 90:10). Yield, 37%; ^{1}H NMR (270 MHz, DMSO-d_6) 6.94 (1H, d, J 8.6 Hz), 7.23 (1H, m), 7.52 (2H, m), 7.65 (3H, m), 7.93 (1H, br-s), 8.03 (2H, d, J 8.4 Hz), 8.25 (1H, s); MS (FAB, Neg) m/z 422 $(M-H)^-$; HRMS (FAB, Neg) $C_{21}H_{12}NO_7S$: calculated 422.0334, found m/z 422.0334 $(M-H)^-$.

2-(4-Ethylamino-3-Nitrobenzoyl)Benzoic Acid (KI-107)

A mixture of 85 mg of KI-102 and 1.2 ml of ethylamine (2.0 M solution in tetrahydrofuran) and 76 mg of DIPEA in 2 ml of 1,4-dioxane was stirred at room temperature for 2 hr and extracted with chloroform. The chloroform extract was purified by a preparative medium pressure liquid chromatography (YAMAZEN Corp.) on silica gel (chloro-

form). Yield, 74%; ^{1}H NMR (270 MHz, DMSO-d_6) 1.29 (3H, t, J 6.8 Hz), 3.52 (2H, dq, J 5.7 Hz, 6.8 Hz), 7.20 (1H, d, J 9.2 Hz), 7.39 (1H, d, J 6.8 Hz), 7.64–7.74 (2H, m), 7.85 (1H, d, J 9.2 Hz), 8.05 (1H, d, J 7.8 Hz), 8.25 (1H, d, J 1.9 Hz), 8.64 (1H, t, J 5.7 Hz); MS (FAB, Neg) m/z 313 $(M-H)^-$; HRMS (FAB, Neg) $C_{16}H_{13}N_2O_5$: calculated 313.0824, found m/z 313.0835 $(M-H)^-$.

2-(4-Cyclohexylamino-3-Nitrobenzoyl)Benzoic Acid (KI-108)

A mixture of 98 mg of KI-102 and 67 mg of cyclohexylamine and 88 mg of DIPEA in 2 ml of 1,4-dioxane was stirred at room temperature for 2 hr and extracted with chloroform. The chloroform extract was purified by a preparative medium pressure liquid chromatography (YAMAZEN Corp.) on silica gel (chloroform). Yield, 43%; ^{1}H NMR (270 MHz, DMSO-d_6) δ 1.06–1.95 (10H, m), 3.48 (1H, m), 7.19 (2H, m), 7.53 (2H, m), 7.76 (1H, d, J 8.9 Hz), 7.98 (1H, d, J 7.3 Hz), 8.14 (1H, s), 8.29 (1H, d, J 9.5 Hz); MS (FAB, Neg) m/z 367 $(M-H)^-$; HRMS (FAB, Neg) $C_{20}H_{19}N_2O_5$: calculated 367.1294, found m/z 367.1336 $(M-H)^-$.

2-(4-Ethoxy-3-Nitrobenzoyl)Benzoic Acid (KI-109)

A mixture of 71 mg of KI-102 and 0.1 ml of sodium ethoxide (21 wt. % solution in denatured ethyl alcohol) in 2 ml of 1,4-dioxane was stirred at room temperature for 3 hr and extracted with chloroform under acidic conditions. The chloroform extract was purified by a preparative medium pressure liquid chromatography (YAMAZEN Corp.) on silica gel (chloroform:methanol = 90:10). Yield, 55%; ^{1}H NMR (270 MHz, DMSO-d_6) 1.34 (3H, t, J 6.8 Hz), 4.26 (2H, q, J 6.8 Hz), 7.25 (1H, m), 7.39 (1H, d, J 8.9 Hz), 7.56 (2H, m), 7.72 (1H, d, J 9.2 Hz), 7.98 (2H, m); MS (FAB, Neg) m/z 314 $(M-H)^-$; HRMS (FAB, Neg) $C_{16}H_{12}NO_6$: calculated 314.0665, found m/z 314.0679 $(M-H)^-$.

2-(4-Phenoxy-3-Nitrobenzoyl)Benzoic Acid (KI-110)

A mixture of 78 mg of KI-102 and 46 mg of sodium phenoxide trihydrate in 2 ml of 1,4-dioxane was stirred at room temperature for 5 hr and extracted with chloroform under acidic conditions. The chloroform extract was purified by a preparative medium pressure liquid chromatography (YAMAZEN Corp.) on silica gel (chloroform). Yield, 99%; ^{1}H NMR (270 MHz, DMSO-d_6) 7.07 (1H, d, J 8.6 Hz), 7.18 (2H, dd, J 1.4 Hz, 7.8 Hz), 7.27–7.36 (2H, m), 7.46–7.52 (2H, m), 7.57–7.67 (2H, m), 7.79 (1H, br-d, J 8.4 Hz), 8.01 (1H, br-d, J 6.8 Hz), 8.18 (1H, br-s), 8.33 (1H, br-s); MS (FAB, Neg) m/z 362 $(M-H)^-$; HRMS (FAB, Neg) $C_{20}H_{12}NO_6$: calculated 362.0665, found m/z 362.0655 $(M-H)^-$.

Cell Culture

Human fibrosarcoma HT1080 cells and HeLa cells were grown in Dulbecco's modified Eagle's medium (DMEM) supplemented with 10% FCS. HepG2-HP cells, which are stable transfectants of human hepatocellular carcinoma HepG2 cells expressing a high level of recombinant human heparanase [37], were grown in DMEM supplemented with 10% FCS and 50 μg/ml of G418 (Geneticin, Gibco Life Technologies, Grand Island, NY). All cell lines were incubated at 37°C in a humidified atmosphere of 5% CO_2/95% air.

Invasion and Migration Assay

In vitro invasion and migration activities were assessed using the method of Albini et al. [38]. BD BioCoat Matrigel Invasion Chamber and Cell Culture Insert (8 μM pore size, Becton Dickinson Labware, Bedford, MA) were used for invasion and migration assays, respectively. The chambers were placed on 24-well plates. Then, 0.5 ml of tumor cell suspension (5×10^4 cells/ml) in DMEM (0% FCS) was added to the upper layer, and 0.75 ml of DMEM (10% FCS) was added to the lower layer. After adhesion for 1 hr, vehicle, compounds, HS, paclitaxel, normal mouse IgG (Santa Cruz Biotechnology, Santa Cruz, CA), or anti-heparanase antibody (BD Biosciences, San Jose, CA) was added to the upper and lower layers. After incubation for 20 hr at 37°C, the tumor cells and Matrigel on the upper surface of the membrane were completely removed by wiping with cotton swabs. Cells on the lower surface of the membrane were fixed in methanol and stained with crystal violet. Cells from various regions of the membrane were counted, and the inhibition percentage was calculated by the following equation: [inhibition % = 100 − (cell number of the compound-treated experiment)/(cell number of the vehicle-treated experiment) × 100].

Adhesion Assay

The tumor cell suspension in DMEM (0% FCS) was added to 96-well BIOCOAT fibronectin coat plate, human fibronectin cellware 35 mm dishes, collagen IV cellware 35 mm dishes, laminin cellware 35 mm dishes, or poly-D-lysine cellware 35 mm dishes (Becton Dickinson Labware, Bedford, MA). After the addition of vehicle, compounds, HS, RGD peptide, RGD control peptide, or paclitaxel, the plate was incubated at 37°C for 1 hr. After washing the plate with PBS, adhered cells were fixed with glutaraldehyde and stained with crystal violet. Cells from various regions of the wells were then counted, and the inhibition percentage was calculated by the following equation: [inhibition % = 100 − (cell number of the chemical-treated experiment)/(cell number of the vehicle-treated experiment) × 100].

Cell Viability Assay

The viability of tumor cells was measured by the WST-8 {2-(2-methoxy-4-nitrophenyl)-3-(4-nitrophenyl)-5-(2,4-disulfophenyl)-2H-tetrazolium} assay [39]. 0.1 ml of cell suspension (1×10^5 cells/ml) was incubated at 37°C for 12 hr. Cells were treated with vehicle, compounds, HS, or paclitaxel at 37°C for 48 hr. Ten microliters of WST-8 monosodium salt solution (5 mM) (Nacalai Tesque, Kyoto, Japan) was added to the wells, and the mixtures were incubated at 37°C for 2 hr. The absorbance was measured at 450 nm. The growth inhibition percentage was calculated by the following equation: [growth inhibition % = 100 − $(A - B)/(C - B)$ × 100], where A is the absorbance of a chemical-treated experiment, B is the absorbance of cell-free experiment, and C is the absorbance of the vehicle-treated experiment.

Wound Healing Assay

HT1080 cells (5×10^5 cells/6-well plate) were incubated in dishes for 24 hr. An artificial wound was carefully created using a plastic tip to scratch the subconfluent cell monolayer. The medium was changed, the cells were treated with chemicals for 20 hr, and photographs were taken.

Immunofluorescence Staining

HT1080 cells were seeded on glass coverslips at a concentration of 2.5×10^4 cells/well of a 6-well plate for 12 hr in DMEM containing 10% FCS; the cells were then incubated for 24 hr with either vehicle or KI-105. Then, the cells were washed with PBS and fixed with 4% paraformaldehyde at room temperature for 20 min. The cells were washed with PBS and incubated with monoclonal antibody against HS (10E4 epitope, Seikagaku Corp., Tokyo, Japan) at room temperature for 1 hr, followed by incubation with Alexa Fluor 488-labeled goat anti-mouse IgM (Molecular Probes Inc., Eugene, OR) for 1 hr. The cells were washed with PBS and incubated with Alexa Fluor 568 phalloidin (Molecular Probes Inc., Eugene, OR) for 1 hr under dark conditions to visualize the actin cytoskeleton. Monoclonal antibody against human vinculin (SIGMA, St. Louis, MO) was used to visualize focal adhesions. The coverslips were mounted on glass slides and visualized using a fluorescence microscope (Olympus, Tokyo, Japan).

Fluorescence-Activated Cell Sorting (FACS)

HT1080 cells were incubated with vehicle or KI-105 for 48 hr. The cells were collected by centrifugation (1000 rpm, 3 min) and washed with PBS. Then, the cells were incubated with monoclonal antibody against HS (10E4 epitope, Seikagaku Corp., Tokyo, Japan) at 4°C for 30 min, followed by incubation with Alexa Fluor 488-labeled goat anti-mouse IgM (Molecular Probes Inc., Eugene, OR) at 4°C for 30 min. Cell-surface HS expression was analyzed by BD FACSCalibur flow cytometry (BD Biosciences, San Jose, CA).

Matrix Metalloproteinases (MMPs) Inhibition Assay

The inhibitory activities against MMP-2 (gelatinase A, 72 kDa type IV collagenase) or MMP-9 (gelatinase B, 92 kDa type IV collagenase) were assessed using the MMP-2 or MMP-9 Colorimetric Assay Kit for Drug Discovery (BIOMOL Research Laboratories, Inc., Plymouth Meeting, PA). The Enz Chek Gelatinase/Collagenase Assay Kit (Molecular Probe, Inc., Eugene, OR) and a MICROTEST 96-Well Assay Plate, Optilux (Becton Dickinson Labware, Bedford, MA) were used for the *Clostridium* collagenase inhibition assay.

Coagulant Factors Inhibition Assay

A reaction mixture of enzyme, KI-105, and chromogenic substrate in PBS (pH 7.0) was incubated at room temperature for 15 min. The absorbance at 405 nm was measured. The chromogenic substrate S-2222 (Chromogenix Instrumentation Laboratory S.p.A., Milano, Italy) was used for the assays of human factor Xa (Enzyme Research Laboratories, South Bend, IN) and human trypsin (Athens Research and Technology, Athens, GA). The chromogenic substrate S-2238 (Chromogenix Instrumentation Laboratory S.p.A., Milano, Italy) was used for the assay of human α thrombin (Enzyme Research Laboratories, South Bend, IN) [40]. Phenylmethanesulfonyl fluoride (PMSF) was used as the positive control for thrombin, and a trypsin inhibitor from *Glycine max* (soybean, SIGMA, St. Louis, MO) was used as the positive control for factor Xa and trypsin.

Urokinase-Type Plasminogen Activator (uPA) Inhibition Assay

For this assay, an uPA activity assay kit (Chemicon International, Inc., Temecula, CA) was used. The reaction mixture of enzyme, KI-105, and a chromogenic substrate was incubated at 37°C for 48 hr. The absorbance at 405 nm was measured. PMSF was used as the positive control.

Heparanase Inhibition Assay

A heparanase-overexpressing stable cell line (HepG2-HP) was established previously [37]. HepG2-HP cells were washed and collected with cold PBS (pH 6.2), subjected to three cycles of freezing and thawing, and the lysates were stored at −20°C. A mixture of 90 μl of cell lysate (2.0 mg/ml of protein) and 10 μl of HS (10 mg/ml in PBS, pH 6.2) with vehicle or KI-105 was incubated for 24 hr at 37°C. After adding 20 μl of HS sampling solution [glycerol: 8 ml, 5 mg/ml of bromophenol blue: 5 ml, H_2O: 19 ml], 10 μl of the reaction mixture was subjected to SDS-PAGE (20%). Electrophoresed gel was soaked in H_2O for 2 hr to remove SDS. The gel was then stained with 0.5% alcian blue 8GX for 3 hr and de-stained with the 1:2:7 mixture of acetic acid-ethanol-water for 12 hr [41]. Volumes of bands were measured using an MD Scanning Imager equipped with MD ImageQuant Software Version 3.22 (Amersham Biosciences Corp., Piscataway, NJ) for quantification.

Western Blotting

Anti-Cdc42, anti-FAK, and anti-αPAK antibodies were purchased from Santa Cruz Biotechnology (Santa Cruz, CA). Anti-Rac1, anti-Rho, anti-paxillin, anti-ILK, and anti-phosphotyrosine antibodies were purchased from BD Biosciences (San Jose, CA). Anti-NCK and anti-α-tubulin antibodies were purchased from Sigma (St. Louis, MO). HT1080 cells were incubated with vehicle or KI-105 for 20 hr. The cells were washed and collected with cold PBS. After centrifugation at 4000 rpm for 5 min, the supernatant was removed, and 100 μl of lysis buffer (10 mM HEPES, 142.5 mM KCl, 5 mM $MgCl_2$, 1 mM EGTA, 0.2% Nonidet P-40, 0.1% aprotinin, and 1 mM phenylmethylsulfonyl fluoride, pH 7.2) was added to the cells. The cells were lysed at 4°C with sonication. After centrifugation at 15,000 rpm for 15 min, 90 μl of supernatant was added to the 30 μl of loading buffer (42 mM Tris-HCl, pH 6.8, 10% glycerol, 2.3% SDS, 5% 2-mercaptoethanol, and 0.002% bromophenol blue). The mixture was heated at 95°C for 3 min and then subjected to SDS-PAGE. The proteins were transferred to PVDF membranes and immunoblotted with specific antibodies, after which they were detected using SuperSignal West Pico Chemiluminescence Substrate (Pierce, Rockford, IL).

Homology Modeling of Heparanase and Construction of Heparanase/KI-105 Complex

The amino acid sequence alignment of human heparanase and 1,4-β-xylanase from *Penicillium simplicissimum* [EC: 3.2.1.8] was manually carried out using the Homology module of Discover/InsightII program (Accelrys Inc., San Diego, CA), and the structurally conserved regions were defined by referring to the results of database searches and site-directed mutagenesis by M.D. Hulett et al. [24] as follows, i.e., for the amino acid sequence of heparanase/the amino acid sequence of 1,4-β-xylanase: 155–179/52–76, 185–192/82–88, 199–210/102–113, 215–228/122–135, 240–269/147–176, 278–292/190–204, 297–300/211–214, 321–330/219–228, 338–345/233–240, 367–370/248–251, 375–388/263–276, 394–411/285–302. Structure construction and molecular dynamics calculations were carried out by the Biopolymer and Discover3 modules of Discover/InsightII program (Accelrys Inc., San Diego, CA) using the X-ray structure of 1,4-β-xylanase (Protein Data Base entry 1BG4) as a template.

Supplemental Data

Supplemental data including the effect of KI-105 and HPLC-purified KI-105 on the migration and invasion of HT1080 cells, purification data of heparanase and inhibitory activity of KI-105 against semipurified heparanase, and amino acid sequence alignment of heparanase and 1,4-β-xylanase are available at http://www.chembiol.com/cgi/content/full/11/3/367/DC1.

Acknowledgments

The authors would like to thank T. Yamazaki and S. Miyasaka (Taiho Pharmaceutical Co., Ltd.) for the database search and spectral measurements, respectively. This study was supported in part by a Grant-in-Aid from the Ministry of Education, Science, Sports, Culture and Technology of Japan, and the Chemical Biology Project (RIKEN).

Received: August 18, 2003
Revised: December 8, 2003
Accepted: December 12, 2003
Published: March 19, 2004

References

1. Perrimon, N., and Bernfield, M. (2000). Specificities of heparan sulphate proteoglycans in developmental processes. Nature *404*, 725–728.
2. Sasisekharan, R., Shriver, Z., Venkataraman, G., and Narayanasami, U. (2002). Roles of heparan-sulphate glycosaminoglycans in cancer. Nat. Rev. Cancer *2*, 521–528.
3. Blackhall, F.H., Merry, C.L., Davies, E.J., and Jayson, G.C. (2001). Heparan sulfate proteoglycans and cancer. Br. J. Cancer *85*, 1094–1098.
4. Woods, A., and Couchman, J.R. (1998). Syndecans: synergistic activators of cell adhesion. Trends Cell Biol. *8*, 189–192.
5. Filmus, J., and Selleck, S.B. (2001). Glypicans: proteoglycans with a surprise. J. Clin. Invest. *108*, 497–501.
6. Lundmark, K., Tran, P.K., Kinsella, M.G., Clowes, A.W., Wight, T.N., and Hedin, U. (2001). Perlecan inhibits smooth muscle cell adhesion to fibronectin: role of heparan sulfate. J. Cell. Physiol. *188*, 67–74.
7. Bezakova, G., and Ruegg, M.A. (2003). New insights into the roles of agrin. Nat. Rev. Mol. Cell Biol. *4*, 295–308.
8. Mundhenke, C., Meyer, K., Drew, S., and Friedl, A. (2002). Heparan sulfate proteoglycans as regulators of fibroblast growth factor-2 receptor binding in breast carcinomas. Am. J. Pathol. *160*, 185–194.
9. Iozzo, R.V., and San Antonio, J.D. (2001). Heparan sulfate proteoglycans: heavy hitters in the angiogenesis arena. J. Clin. Invest. *108*, 349–355.
10. Ma, Y.Q., and Geng, J.G. (2000). Heparan sulfate-like proteoglycans mediate adhesion of human malignant melanoma A375 cells to P-selectin under flow. J. Immunol. *165*, 558–565.
11. Vlodavsky, I., Bar-Shavit, R., Ishai-Michaeli, R., Bashkin, P., and Fuks, Z. (1991). Extracellular sequestration and release of fibroblast growth factor: a regulatory mechanism? Trends Biochem. Sci. *16*, 268–271.
12. Toyoshima, M., and Nakajima, M. (1999). Human heparanase. Purification, characterization, cloning, and expression. J. Biol. Chem. *274*, 24153–24160.
13. Vlodavsky, I., Friedmann, Y., Elkin, M., Aingorn, H., Atzmon, R., Ishai-Michaeli, R., Bitan, M., Pappo, O., Peretz, T., Michal, I., et al. (1999). Mammalian heparanase: gene cloning, expression and function in tumor progression and metastasis. Nat. Med. *5*, 793–802.
14. Hulett, M.D., Freeman, C., Hamdorf, B.J., Baker, R.T., Harris, M.J., and Parish, C.R. (1999). Cloning of mammalian heparan-

ase, an important enzyme in tumor invasion and metastasis. Nat. Med. *5*, 803–809.
15. Kussie, P.H., Hulmes, J.D., Ludwig, D.L., Patel, S., Navarro, E.C., Seddon, A.P., Giorgio, N.A., and Bohlen, P. (1999). Cloning and functional expression of a human heparanase gene. Biochem. Biophys. Res. Commun. *261*, 183–187.
16. Tumova, S., Woods, A., and Couchman, J.R. (2000). Heparan sulfate proteoglycans on the cell surface: versatile coordinators of cellular functions. Int. J. Biochem. Cell Biol. *32*, 269–288.
17. Kjellen, L., and Lindahl, U. (1991). Proteoglycans: structures and interactions. Annu. Rev. Biochem. *60*, 443–475.
18. Lipinski, C.A., Lombardo, F., Dominy, B.W., and Feeney, P.J. (2001). Experimental and computational approaches to estimate solubility and permeability in drug discovery and development settings. Adv. Drug Deliv. Rev. *46*, 3–26.
19. Kraszni, M., Banyai, I., and Noszal, B. (2003). Determination of conformer-specific partition coefficients in octanol/water systems. J. Med. Chem. *46*, 2241–2245.
20. Yang, W., Lin, Q., Guan, J.L., and Cerione, R.A. (1999). Activation of the Cdc42-associated tyrosine kinase-2 (ACK-2) by cell adhesion via integrin beta1. J. Biol. Chem. *274*, 8524–8530.
21. Stetler-Stevenson, W.G., Aznavoorian, S., and Liotta, L.A. (1993). Tumor cell interactions with the extracellular matrix during invasion and metastasis. Annu. Rev. Cell Biol. *9*, 541–573.
22. Vassalli, J.D., and Pepper, M.S. (1994). Tumour biology. Membrane proteases in focus. Nature *370*, 14–15.
23. Sato, H., Takino, T., Okada, Y., Cao, J., Shinagawa, A., Yamamoto, E., and Seiki, M. (1994). A matrix metalloproteinase expressed on the surface of invasive tumour cells. Nature *370*, 61–65.
24. Hulett, M.D., Hornby, J.R., Ohms, S.J., Zuegg, J., Freeman, C., Gready, J.E., and Parish, C.R. (2000). Identification of active-site residues of the pro-metastatic endoglycosidase heparanase. Biochemistry *39*, 15659–15667.
25. Bar-Ner, M., Eldor, A., Wasserman, L., Matzner, Y., Cohen, I.R., Fuks, Z., and Vlodavsky, I. (1987). Inhibition of heparanase-mediated degradation of extracellular matrix heparan sulfate by non-anticoagulant heparin species. Blood *70*, 551–557.
26. Irimura, T., Nakajima, M., and Nicolson, G.L. (1986). Chemically modified heparins as inhibitors of heparan sulfate specific endo-beta-glucuronidase (heparanase) of metastatic melanoma cells. Biochemistry *25*, 5322–5328.
27. Miao, H.Q., Elkin, M., Aingorn, E., Ishai-Michaeli, R., Stein, C.A., and Vlodavsky, I. (1999). Inhibition of heparanase activity and tumor metastasis by laminarin sulfate and synthetic phosphorothioate oligodeoxynucleotides. Int. J. Cancer *83*, 424–431.
28. Saiki, I., Murata, J., Nakajima, M., Tokura, S., and Azuma, I. (1990). Inhibition by sulfated chitin derivatives of invasion through extracellular matrix and enzymatic degradation by metastatic melanoma cells. Cancer Res. *50*, 3631–3637.
29. Parish, C.R., Freeman, C., Brown, K.J., Francis, D.J., and Cowden, W.B. (1999). Identification of sulfated oligosaccharide-based inhibitors of tumor growth and metastasis using novel in vitro assays for angiogenesis and heparanase activity. Cancer Res. *59*, 3433–3441.
30. Takahashi, S., Kuzuhara, H., and Nakajima, M. (2001). Design and synthesis of a heparanase inhibitor with pseudodisaccharide structure. Tetrahedron *57*, 6915–6926.
31. Nobes, C.D., and Hall, A. (1995). Rho, rac, and cdc42 GTPases regulate the assembly of multimolecular focal complexes associated with actin stress fibers, lamellipodia, and filopodia. Cell *81*, 53–62.
32. Nobes, C.D., and Hall, A. (1999). Rho GTPases control polarity, protrusion, and adhesion during cell movement. J. Cell Biol. *144*, 1235–1244.
33. Simizu, S., Ishida, K., Wierzba, M.K., Sato, T.A., and Osada, H. (2003). Expression of heparanase in human tumor cell lines and human head and neck tumors. Cancer Lett. *193*, 83–89.
34. Woods, A., and Couchman, J.R. (1994). Syndecan 4 heparan sulfate proteoglycan is a selectively enriched and widespread focal adhesion component. Mol. Biol. Cell *5*, 183–192.
35. Wilcox-Adelman, S.A., Denhez, F., and Goetinck, P.F. (2002). Syndecan-4 modulates focal adhesion kinase phosphorylation. J. Biol. Chem. *277*, 32970–32977.
36. Thodeti, C.K., Albrechtsen, R., Grauslund, M., Asmar, M., Larsson, C., Takada, Y., Mercurio, A.M., Couchman, J.R., and Wewer, U.M. (2003). ADAM12/syndecan-4 signaling promotes beta 1 integrin-dependent cell spreading through protein kinase Calpha and RhoA. J. Biol. Chem. *278*, 9576–9584.
37. Simizu, S., Ishida, K., Wierzba, M.K., and Osada, H. (2004). Secretion of heparanase protein is regulated by glycosylation in human tumor cell lines. J. Biol. Chem. *279*, 2697–2703.
38. Albini, A., Iwamoto, Y., Kleinman, H.K., Martin, G.R., Aaronson, S.A., Kozlowski, J.M., and McEwan, R.N. (1987). A rapid in vitro assay for quantitating the invasive potential of tumor cells. Cancer Res. *47*, 3239–3245.
39. Isobe, I., Michikawa, M., and Yanagisawa, K. (1999). Enhancement of MTT, a tetrazolium salt, exocytosis by amyloid beta-protein and chloroquine in cultured rat astrocytes. Neurosci. Lett. *266*, 129–132.
40. Nishida, H., Miyazaki, Y., Mukaihira, T., Saitoh, F., Fukui, M., Harada, K., Itoh, M., Muraoka, A., Matsusue, T., Okamoto, A., et al. (2002). Synthesis and evaluation of 1-arylsulfonyl-3-piperazinone derivatives as a factor Xa inhibitor II. Substituent effect on biological activities. Chem. Pharm. Bull. (Tokyo) *50*, 1187–1194.
41. De Vouge, M.W., Yamazaki, A., Bennett, S.A., Chen, J.H., Shwed, P.S., Couture, C., and Birnboim, H.C. (1994). Immunoselection of GRP94/endoplasmin from a KNRK cell-specific lambda gt11 library using antibodies directed against a putative heparanase amino-terminal peptide. Int. J. Cancer *56*, 286–294.